ACS OMEGA

Open Access

http://pubs.acs.org/journal/acsodf

Article

CBD-Loaded Nanostructured Lipid Carriers: Optimization, Characterization, and Stability

Yang Xie,* Peng Li, Dong Fu, Fan Yang, Xin Sui, Bo Huang, Jiaying Liu, and Jialong Chi

Cite This: *ACS Omega* 2024, 9, 40632−40643

Read Online

ACCESS | Metrics & More | Article Recommendations | Supporting Information

ABSTRACT: Cannabidiol (CBD) has demonstrated its potential to enhance depression treatment through various biological pathways. However, the application potential of CBD is significantly impeded by its polymorphic nature, limited water solubility, and hepatic first-pass metabolism. To improve chemical stability and water solubility, nanostructured lipid carriers loaded with CBD (CBD-NLCs) were developed using a hot-melt emulsification method and optimized by response surface methodology (RSM). The process parameters were optimized using a four-factor and three-level Box−Behnken experimental design consisting of 29 experiments. The CBD-NLCs were formulated and characterized, demonstrating desirable properties, including a mean particle size of 54.33 nm, a PDI value of 0.118, a zeta potential of −29.7 mV, and an impressive encapsulation efficiency rate of 87.58%. The nanoparticles were found to possess an approximately spherical shape, as revealed by scanning and transmission electron microscopy. The stability studies have demonstrated that CBD-NLCs effectively mitigated the photodegradation of CBD and exhibited a stable behavior for 42 days when stored. The CBD-NLCs displayed a biphasic release profile characterized by an initial burst release (over 50% of CBD released within 20 min) followed by a subsequent gradual and sustained release, aligned with first-order kinetics and Fickian diffusion. These findings demonstrate the potential suitability of this formulation as a carrier for CBD in food fortification and pharmaceutical applications.

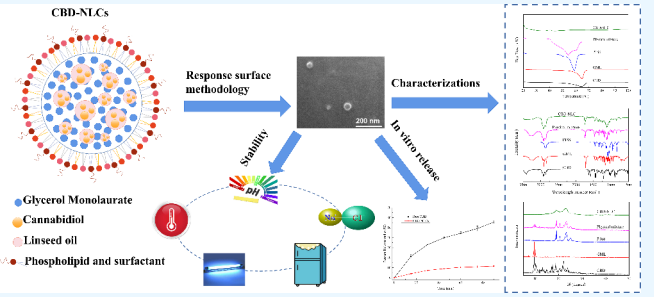

1. INTRODUCTION

Depression is a common disorder that affects millions of people worldwide and usually coexists with various other symptoms, such as anxiety, insomnia, anorexia, pain, and palpitation, among others.[1,2] Despite being primarily considered a psychological illness, depression involves biological alterations in the body. It has been reported that enhancing the endocannabinoid system (ECS) signaling can effectively ameliorate depression-related dysfunction, and targeting ECS for depression treatment garnered significant attention among researchers.[3−6] Cannabidiol (CBD), a naturally occurring nonpsychoactive compound derived from cannabis, has demonstrated potential in numerous clinical and preclinical studies to ameliorate depression, Alzheimer's disease, Parkinson's disease, sleep disorders, and psychotic disorders through multiple biological pathways.[7−13] Consequently, CBD has emerged as a promising therapeutic option for patients with depression due to its favorable safety profile and tolerability in humans.[14−16] Usually, oral ingestion is preferred for CBD administration. However, because of its polymorphic nature, poor water solubility (0.1 μg/mL),[17] and first-pass effect, the oral bioavailability of CBD is limited (6−13%).[18−21] Therefore, it is imperative to develop a water-soluble formulation of CBD to enhance its oral bioavailability and efficacy.

Over the past few years, numerous drug delivery systems have been developed to improve the aqueous solubility and oral bioavailability of CBD, including transdermal delivery systems, transmucosal delivery systems, self-emulsifying delivery systems, and other novel preparation delivery technologies.[22,23] The transdermal delivery system offers the advantage of controlled release drug delivery to the bloodstream, bypassing first-pass metabolism in the liver and enhancing therapeutic efficacy.[24] However, the transdermal transport of CBD exhibits a sluggish rate and necessitates an extended duration to attain the desired concentration.[25] The transmucosal delivery systems provide rapid drug absorption to achieve effective concentrations, but the variability in CBD absorption between individuals is high due to its accumulation in mucosal tissue and subsequent swallowing into the gastrointestinal tract though saliva.[26,27] The self-emulsifying delivery systems can enhance the permeability of drugs across the intestinal epithelial cell membrane, thereby

Received: May 20, 2024
Revised: August 6, 2024
Accepted: September 11, 2024
Published: September 19, 2024

augmenting their bioavailability, but they still face challenges related to stability, complexity, and safety.[28,29] To enhance CBD solubility for improved absorption, novel preparation technologies such as dispersions, eutectics, and nanoparticles have been developed.[30] Nevertheless, the challenges of achieving a high excipient ratio and low drug loading and overcoming first-pass metabolism persist. The current challenges surrounding CBD delivery carriers have not yet been fully addressed. It is crucial to select an appropriate carrier based on its compatibility with CBD for an effective drug delivery system. Enhancing the stability and solubility of CBD remains a primary concern for improving absorption at the gastrointestinal level.

Nanostructured lipid carriers (NLCs), serving as efficient and targeted vehicles for drug delivery, are formulated by mixing solid and liquid lipids, which enable effective loading of active ingredients into their structure.[31−34] NLCs have multiple advantages, such as nontoxicity, storage stability, high drug loading capacity, protection of sensitive drug, and enhanced bioavailability, making them a highly attractive system for oral administration of various active ingredients.[35] Moreover, NLCs exhibit solid-state characteristics at both room and body temperatures, which demonstrate enhanced drug loading efficiencies and prevent drug ejection and oxidation during storage.[36,37] Additionally, coadministration of drugs with lipids promotes lymphatic absorption and direct entry into the systemic circulation to circumvent the first-pass metabolism by the liver.[38,39] Furthermore, NLCs offer ease of manufacturing without the need for organic solvents in preparation. The impact of NLC delivery systems, which are considered a critical drug delivery strategy, is steadily expanding. In addition, NLCs can enhance the solubility of CBD in the intestinal lumen, thereby offering an additional mechanism to augment its bioavailability.[40,41] Therefore, it is necessary to further research and explore the application and effectiveness of CBD-NLCs in foods and pharmaceuticals.

Despite the significant advantages offered by NLCs, further research is essential to investigate the components and formulation design. Given the multitude of lipids, phospholipids, and surfactants available, the selection of ingredients becomes a cumbersome process. The particle size and encapsulation efficiency (EE) of NLCs are the main characteristics to be considered, which are related to greater surface area, minimal drug loss, and controlled drug release. In recent years, several CBD-NLCs with different formulations were investigated. Morakul et al. studied the effects of formulation (cetyl palmitate as a solid lipid stabilized with Tego Care 450 or poloxamer 188) compositions on the performance of CBD-NLCs. They found that the physicochemical characteristics of CBD-NLCs were influenced by the specific types of surfactants and lipids used, and packaging CBD showed the potential for reducing the cytotoxicity.[42] Vardanega et al. discovered that NLCs can serve as an appropriate carrier for either CBD-rich extract or isolate CBD.[43] Therefore, it is still a challenging and economically feasible approach to fabricate CBD-NLCs with high reproducibility at the nanoscale.

The aim of this study was the design and optimization of CBD-loaded nanostructured lipid carriers (CBD-NLCs) with smaller particle size, narrow size distribution, and higher encapsulation efficiency as well as good chemical stability and water solubility. The particle size, polydispersity index (PDI), zeta potential, and encapsulation efficiency of each formulation were evaluated. Additionally, the crystallization behavior and physicochemical stability of the resulting optimal formulation were investigated. To further explore the application performance of CBD-NLCs, the encapsulation efficiency, photothermal stability, and in vitro release of CBD were evaluated. The findings from this study will provide essential insights into the development and application of CBD-NLCs in functional foods or pharmaceutical applications.

2. EXPERIMENTAL MATERIALS AND METHODS

2.1. Reagents. CBD was purchased from Shanghai Saihan Technology Co. Ltd. Glycerol monolaurate (GML), linseed oil (LO), and Tween 60 were obtained from Shanghai Aladdin Biochemical Technology Co. Ltd. Kolliphor P188 was bought from Nanjing Weil Chemical Co. Ltd. Egg yolk lecithin (EYL) was purchased from Beijing Solarbio Technology Co. Ltd. All other chemicals used were analytical grade.

2.2. Preparation of the CBD-NLCs. Prior to the actual preparation, a preliminary screening was conducted for the solid lipid, liquid lipid, and surfactant, which were described in the experimental method in the Supporting Information. CBD-NLCs were prepared using a hot-melt emulsification method. The GML, LO, and CBD were heated at 68 °C and mixed to form the liquid phase. The aqueous phase containing the surfactant and deionized water was heated at the same temperature until the mixture became a clear gel. The aqueous phase was added slowly into the lipid phase under continuous stirring of 1000 rpm to produce the pre-emulsion. After stirring for 30 min, the pre-emulsion was sonicated by an ultrasonic probe with a constant cycle for 3 min (4 s on and 7 s off). Finally, samples were placed in an ice bath for 15 min to form lipid carriers with a nanostructure and then stored at room temperature until further characterization. The blank NLCs were prepared as described above without CBD in the liquid phase.

2.3. Experimental Design. For producing the optimized NLCs, the experiment of RSM design was used, and the resulting data were analyzed by using the Design Expert 11.0 software. A Box−Behnken design (BBD) consisting of a three-level and four-factor experimental model with 29 runs was selected to optimize the formulation procedure. Four variables, namely, solid−liquid lipid ratio (A), lipid concentration (B), surfactant concentration (C), and CBD concentration (D), were identified as independent variables for optimization based on the results of previous single-factor experiments. The dependent variables for the study included particle size (Y1), PDI (Y2), and encapsulation efficiency (Y3). The adequacy of the fitted model was statistically analyzed by ANOVA, and contour plots and 3D surface graphs were generated to represent the response values. The dependent and independent variables used in the experiments are listed in Table 1.

The obtained data were subject to statistical analysis. The p-value, the p-value of lack of fit, the regression coefficient (R^2), the adjusted R^2, and other parameters of the model were analyzed, and finally, the suitable best-fitting model was selected. To verify the applicability of the quadratic equation to predict the optimal formula, three experiments were carried out under optimal conditions.

2.4. Characterizations of NLCs. *2.4.1. Particle Size, PDI, and Zeta Potential.* A dynamic light scattering (DLS) instrument (Nano ZS, Malvern Instruments, UK) was employed to determine the mean of particle size (Z-average), PDI, and zeta potential of NLCs. The samples were diluted in a 1:50 ratio and kept standing for 10 min to avoid multiple scatterings of light caused by a high concentration of particles. The measurements

https://doi.org/10.1021/acsomega.4c04771
ACS Omega 2024, 9, 40632−40643

Table 1. Box−Behnken Design with the List of Dependent and Independent Variables

variable, unit	factors	level		
	X	−1	0	1
independent variables				
solid−liquid lipid ratio (w/w)	A	1	1.5	2
lipid concentration (w/v)	B	0.75	1.5	2.25
surfactant concentration (w/v)	C	2	3	4
CBD concentration (w/v)	D	0.8	1.2	1.6
dependent variables				optimized response
particle size (nm)	Y1			minimize
PDI	Y2			minimize
EE (%)	Y3			maximize

were conducted in triplicate and repeated three times at room temperature (25 °C).

2.4.2. Particle Morphology. The morphology of the optimized CBD-NLCs was observed with scanning electron microscopy (SEM, SU5000, Hitachi Limited, Japan) and transmission electron microscopy (TEM, JSM-IT800, JEOL, Japan). The CBD-NLCs were appropriately diluted with deionized water. A drop of the dispersion sample was dried on aluminum foil and desiccated prior to SEM observation. Another drop was deposited onto 200-mesh carbon copper grids and air-dried at room temperature for TEM analysis.

2.4.3. HPLC Analysis and Entrapment Efficiency (EE). The free drug was separated from the drug entrapped in the NLCs using a previously described ultrafiltration/centrifugation method.[44] A dispersion of CBD-NLCs, approximately 2 mL in volume, was loaded into the upper chamber of a centrifugal filter tube and then centrifuged at 12,000 rpm for 15 min (20 °C). The concentration of CBD in the supernatant was analyzed by HPLC (Agilent1260 Infinity, Agilent, USA).

A mixture of acetonitrile and water (21:79) was used as the mobile phase with a flow rate of 1 mL/min. CBD was estimated at 220 nm using the reversed-phase Symmetry-C18 (250 × 4.6 mm, 3.5 μm) HPLC column at 25 °C. The CBD standard was diluted with mobile phase to obtain 0.1−20 μg/mL standard solution and analyzed immediately. Linear regression analysis was performed using the Origin Pro 9.1 software to determine the slope, intercept, and correlation coefficient (R^2). A calibration curve with a linear regression equation (Figure S1) was prepared, whereas x and y are the concentration (μg/mL) and area, respectively. The percent encapsulation efficiency was estimated as per eq 1:

$$\text{EE\%} = \frac{(\text{total amount of CBD} - \text{free CBD})}{\text{total amount of CBD}} \times 100 \quad (1)$$

2.4.4. Fourier Transformed Infrared Spectroscopy (FTIR). The FTIR spectrum of the samples was obtained by the KBr pellet method using FTIR spectroscopy (iS50 FT-IR, Nicolet, UK) at room temperature. The measurements were recorded in the range of 500−3500 cm^{-1}.

2.4.5. Differential Scanning Calorimetry (DSC). Thermal properties of the samples was performed using DSC measurements (Q20, TA Instruments, USA). Samples of CBD-NLCs, P188, GML, CBD, and a physical mixture were weighed and placed in sealed aluminum pans. DSC curves were recorded from 20 to 250 °C at a heating rate of 10 °C/min under a nitrogen atmosphere (50 mL/min).

2.4.6. Powder X-ray Diffraction (XRD). The PXRD $\theta/2\theta$ analysis was performed using powder X-ray diffractometer (X'Pert3 Powder, Malvern, England) under the following conditions: room temperature (293 K), Cu Kα radiation (1.5418 Å) generated at 40 kV and 40 mA, and a scan speed of 5°/min. The diffraction data were obtained at 2θ diffraction angles between 5 and 90° with a step size of 0.02626°.

2.5. Stability of CBD-NLCs. *2.5.1. Ionic and pH Stability.* Freshly prepared CBD-NLCs were added to different concentrations of NaCl and $CaCl_2$, resulting in final salt concentrations of 0, 10, 25, 50, 100, 200, and 300 mmol/L. Subsequently, the samples were incubated at room temperature for 1 h before analyzing the particle size and PDI.

Likewise, the CBD-NLCs were mixed with phosphate buffer solutions of varying pH values and incubated at room temperature for 30 min. Subsequently, all samples were characterized by particle size, PDI, and EE. The present release ratio of the samples was calculated by using eq 2:

$$\text{Release ratio\%} = \left(1 - \frac{\text{EE}_\text{p}}{\text{EE}_0}\right) \times 100 \quad (2)$$

where EE_p is the EE% of the sample at a specific condition and EE_0 is the EE% of the sample at the initial time.

2.5.2. UV-Light Stability. To examine the UV-light stability of CBD-NLCs, the free CBD and encapsulated CBD were placed in a controlled lightbox at room temperature and illuminated with UV-light at 365 nm. The samples were collected at different time points (0, 15, 30, 45, 60, 75, and 90 min) to measure the release ratio at each time point.

2.5.3. Thermal Stability. Freshly prepared CBD-NLCs were exposed to different temperature conditions (4, 25, 37, 60, and 80 °C) for 90 min individually. Then, all samples were immediately transferred to an ice bath for rapid cooling to prevent any further heat-induced CBD release. The particle size, PDI, and release ratio were investigated. The EE% was calculated using eq 1, whereas the release ratio was calculated using eq 2.

2.5.4. Storage Stability. The storage stability of freshly prepared CBD-NLCs was assessed over a period of 42 days, during which the samples were stored at both 4 °C and room temperature (20 ± 3 °C). The particle size, PDI, and release ratio were tested at different time points (0, 4, 7, 14, 21, 28, 35, and 42 days).

2.6. In Vitro Release Study. The in vitro release of CBD in NLCs was investigated referring to the previous literature with some modification.[45] The CBD-NLCs and CBD were placed in phosphate-buffered saline (PBS, 20 mM, pH 6.8) containing P188 (2%, w/v) in a thermostatic shaker (37 ± 1 °C) for 90 min. One milliliter of supernatant was collected at 5, 10, 20, 30, 60, and 90 min and replaced with an equal volume of buffer. Subsequently, the samples were filtered through 0.2 μm membranes, and the amount of CBD released was determined by the aforementioned HPLC method. The cumulative drug release rate (Q) was determined at each time point using the following calculation:

$$Q\ (\%) = (V_0 \times C_t + V \times \sum_{n=1}^{t-1} C_t) \times 100\% \times M^{-1} \quad (3)$$

where V_0 is the total volume of the release medium (mL), C_t denotes the CBD concentration at different time points (μg/

https://doi.org/10.1021/acsomega.4c04771
ACS Omega 2024, 9, 40632−40643

Table 2. Observed Responses of Trial Experiments as per the Box−Behnken Design Matrix

exp.	A	B	C	D	Y1	Y2	Y3
1	0	1	1	0	60.73 ± 0.85	0.148 ± 0.005	84.05 ± 1.22
2	0	−1	−1	0	101.2 ± 3.02	0.171 ± 0.004	80.40 ± 0.38
3	0	−1	1	0	37.90 ± 0.87	0.185 ± 0.011	83.63 ± 1.54
4	−1	−1	0	0	50.71 ± 0.32	0.213 ± 0.007	79.31 ± 4.37
5	0	−1	0	1	66.17 ± 1.23	0.161 ± 0.004	83.49 ± 0.86
6	1	1	0	0	55.19 ± 1.42	0.126 ± 0.008	85.38 ± 1.28
7	1	−1	0	0	55.50 ± 2.05	0.155 ± 0.005	83.22 ± 2.84
8	−1	0	−1	0	69.15 ± 0.77	0.126 ± 0.008	83.34 ± 1.96
9	0	1	0	−1	64.80 ± 2.14	0.142 ± 0.010	89.35 ± 2.12
10	0	0	−1	1	90.08 ± 3.05	0.144 ± 0.006	82.53 ± 2.04
11	1	0	−1	0	112.30 ± 0.54	0.175 ± 0.012	90.24 ± 0.57
12	0	0	1	1	51.35 ± 0.72	0.137 ± 0.007	84.89 ± 1.28
13	0	0	1	−1	37.50 ± 1.63	0.168 ± 0.004	83.96 ± 2.18
14	1	0	0	1	85.71 ± 2.57	0.134 ± 0.005	86.33 ± 3.05
15	0	−1	0	−1	38.87 ± 1.24	0.178 ± 0.005	78.08 ± 1.76
16	−1	0	0	−1	51.31 ± 1.61	0.129 ± 0.003	81.63 ± 2.21
17	1	1	0	0	85.71 ± 2.33	0.192 ± 0.013	90.17 ± 0.88
18	0	0	0	0	52.23 ± 0.27	0.131 ± 0.003	87.82 ± 1.37
19	0	0	0	0	50.37 ± 1.02	0.126 ± 0.008	86.05 ± 2.42
20	−1	0	1	0	40.46 ± 1.36	0.149 ± 0.005	82.32 ± 3.55
21	0	0	0	0	60.09 ± 0.86	0.124 ± 0.012	87.41 ± 0.89
22	0	0	0	0	56.37 ± 2.41	0.129 ± 0.005	86.27 ± 2.36
23	1	0	0	−1	54.41 ± 1.32	0.179 ± 0.011	86.96 ± 0.74
24	0	0	0	0	52.20 ± 0.96	0.140 ± 0.006	87.27 ± 2.16
25	0	1	0	1	61.27 ± 1.22	0.139 ± 0.003	84.13 ± 0.67
26	1	0	1	0	48.37 ± 2.31	0.162 ± 0.007	86.85 ± 1.87
27	0	1	−1	0	95.80 ± 3.87	0.145 ± 0.005	88.92 ± 1.68
28	0	0	−1	−1	93.82 ± 0.54	0.120 ± 0.003	87.21 ± 2.56
29	−1	0	0	1	47.23 ± 0.73	0.136 ± 0.012	81.88 ± 3.36

Table 3. Summary of Regression Coefficients, *p*-Values, and Fitting Parameters' Model of Responses

response model	Y1: particle size (nm)		Y2: PDI		Y3: EE (%)	
suggested model	quadratic		quadratic		quadratic	
model *p*-value	<0.0001		<0.0001		<0.0001	
R^2	0.9775		0.9444		0.9613	
adj. R^2	0.9550		0.8888		0.9225	
pred. R^2	0.8932		0.7207		0.8131	
adeq prec.	25.0117		15.8966		18.5467	
C.V.%	6.81		5.26		1.02	
lack of fit *p*-value	0.4472		0.2847		0.3980	
source	*p*-value	coefficient estimate	*p*-value	coefficient estimate	*p*-value	coefficient estimate
A	<0.0001	10.07	0.0007	0.0098	<0.0001	2.49
B	0.0005	5.51	<0.0001	−0.0143	<0.0001	2.82
C	<0.0001	−23.84	0.0265	0.0057	0.0369	−0.5783
D	0.0010	5.09	0.0327	−0.0054	0.2114	−0.3283
AB	0.0465	4.67	<0.0001	0.0310	0.6203	0.2200
AC	0.0010	−8.81	0.0392	−0.0090	0.1940	−0.5925
AD	0.0010	8.85	0.0054	−0.0130	0.6203	−0.2200
BC	0.0052	7.06	0.4985	−0.0027	0.0004	−2.02
BD	0.0029	−7.71	0.3915	0.0035	<0.0001	−2.66
CD	0.0588	4.40	0.0037	−0.0137	0.0061	1.40
A^2	0.2583	1.98	0.0003	0.0148	0.0363	−0.7895
B^2	0.0253	4.20	<0.0001	0.0246	0.0002	−1.73
C^2	<0.0001	13.19	0.0117	0.0090	0.0591	−0.7008
D^2	0.4975	1.17	0.7228	0.0011	0.0002	−1.69

mL), V is the sampling volume, and M refers to the total mass of the CBD (mg).

The kinetics of cumulative CBD release from CBD-NLCs was studied utilizing zero-order, first-order, Higuchi, and Ritger−Peppas models (eqs S1−S4).

https://doi.org/10.1021/acsomega.4c04771
ACS Omega 2024, 9, 40632−40643

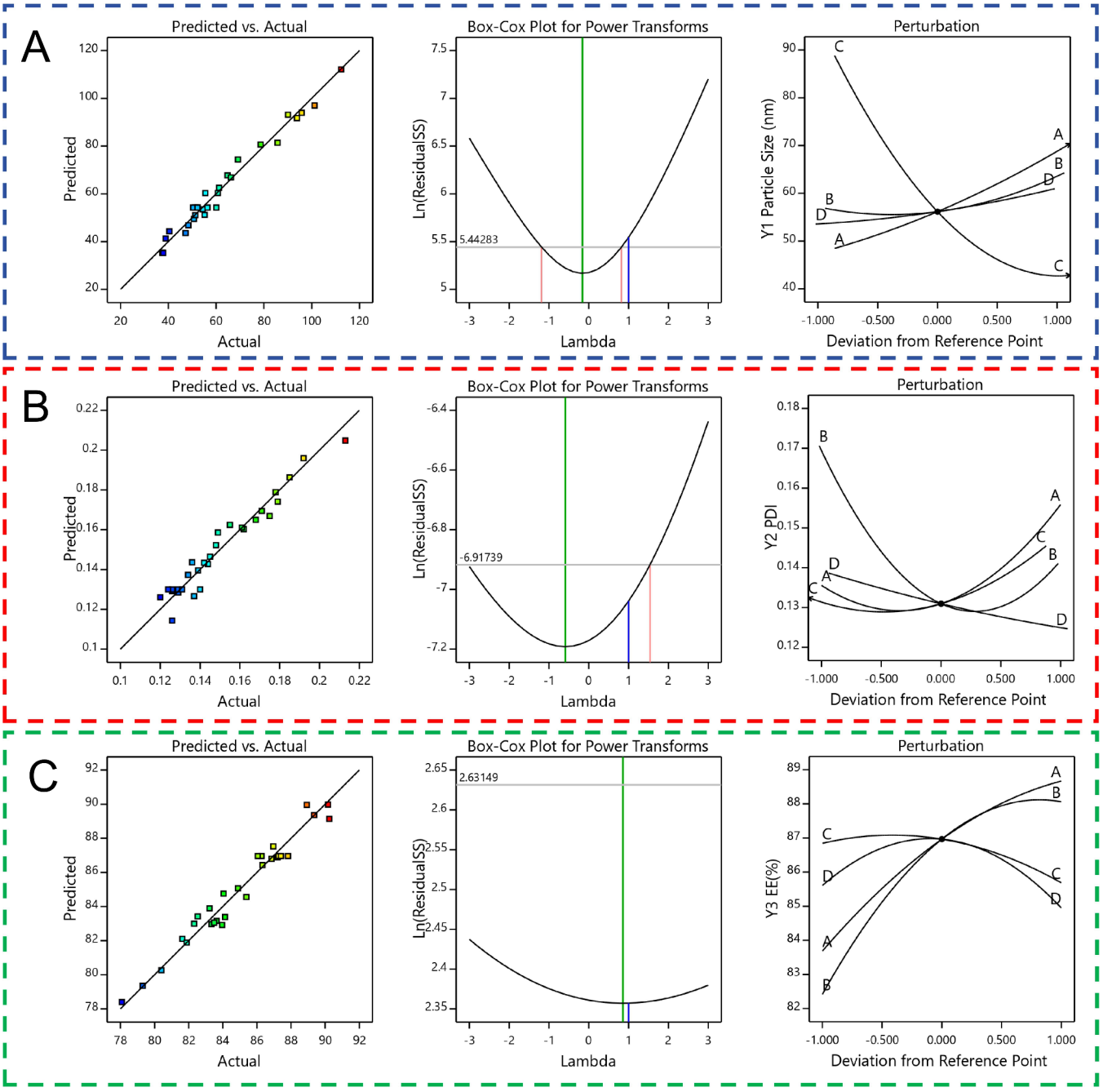

Figure 1. Comparison between predicted and actual vales, Box−Cox plot, and two-dimensional perturbation plot for different dependent variables Y: (A) particle size; (B) PDI; and (C) EE.

3. RESULTS AND DISCUSSION

GML was selected as the solid lipid due to its ability to reduce the particle size of CBD-NLCs and decrease the instability caused by creaming or sedimentation resulting from Brownian motion (Table S1). Furthermore, GML is a naturally occurring compound known for its antibacterial properties in the breast milk of various animals, and its antibacterial effect is not affected by pH value. Additionally, GML can inhibit inflammation in epithelial cells. LO was selected as the liquid lipid based on its significant ability to reduce PDI, resulting in a more uniform particle size distribution of NLCs (Table S2). The compound emulsifier (Tween 60/P188/EYL = 6:3:1) can maintain stable zeta potential and high EE% (Table S3).

3.1. Box−Behnken Design and Data Analysis.

The levels of each variable were determined based on the previous experimental findings. Table 2 presents the results of 29 tests performed using a four-factor, three-level design. All of the results from RSM-BBD were fitted into a second-order quadratic (Table 3), and the rationality of the model was verified by analysis of variance, lack of fit, and regression coefficient (R^2) values. The Adeq Precision of Y1, Y2, and Y3 is greater than 4, indicating adequate signals, respectively. The difference between Pred. R^2 and is Adj. R^2 is less than 0.2, meaning that the regression model can fully explain the process. If it is more than 0.2, it indicates a large block effect or a possible problem with the model. C.V.% is less than 10, indicating the reproducibility, high reliability, and accuracy of the obtained results.

https://doi.org/10.1021/acsomega.4c04771
ACS Omega 2024, 9, 40632−40643

3.1.1. Effects on Particle Size. The size and distribution of the particle size play a crucial role in determining the stability, solubility, dissolution, and permeability of the nanoformulation. The average size of CBD-NLCs varied from 37.5 ± 1.63 to 112.30 ± 0.54 nm across all 29 experimental runs conducted. Figure S2 shows a three-dimensional (3D) surface response of the variable's impact on particle size. The influence of different variables on the particle size of CBD-NLCs can be demonstrated by the software generated quadratic equation as follows:

$$\begin{aligned}\text{Mean particle size} = {} & + 54.25 + 10.07A + 5.51B \\ & - 23.84C + 5.09D + 4.67AB \\ & - 8.81AC + 8.85AD + 7.06BC \\ & - 7.71BD + 4.4CD + 1.98A^2 \\ & + 4.2B^2 + 13.19C^2 + 1.17D^2\end{aligned}$$

The coefficients with positive signs indicate synergism, whereas the coefficients with negative signs indicate antagonism. The regression coefficient value was high ($R^2 = 0.9803$), and the lack of fit was not significant, which indicated that the model adequately predicts the particle size of CBD-NLCs. According to the predicted and actual fitting lines in Figure 1A, the closer to a line, the better fitting effect will be. The Box−Cox transform is used in case continuous response variables do not meet the normal distribution. The Box−Cox transform can reduce unobserved errors and correlation of prediction variables to a certain extent when continuous response variables do not meet the normal distribution. When lambda is −0.16, the Box−Cox curve of power transformation reaches the minimum value; that is, it can reduce the correlation effect of inconvenient to predict dimension parameters and observation errors, and improve the accuracy of data processing. A perturbation plot was used to describe the influence of individual variable on particle size. The results showed that all the variables had a significant effect on the particle size. The influence of each variable on particle size is as follows: C (surfactant concentration) > A (solid−liquid lipid ratio) > B (lipid concentration) > D (CBD concentration). Surfactant concentration plays a major role in particle size. As the C increased, the particle size decreased obviously. Conversely, as the A, B, and D increased, the particle size was increased. In addition, there were some synergistic and antagonistic effects among the variables.

3.1.2. Effects on PDI. The PDI serves as an important index of the physical stability of NLCs, with a PDI value below 0.3 generally denoting uniform dispersion within the system. The PDI range of CBD-NLCs varied from 0.120 ± 0.003 to 0.192 ± 0.013 in all 29 runs. Figure S3 shows a 3D surface response of the variable's impact on PDI. The quadratic equations mentioned below show the influence of variables on the PDI of CBD-NLCs:

$$\begin{aligned}\text{PDI} = {} & + 0.13 + 0.0098A - 0.0143B + 0.0057C \\ & - 0.0054D + 0.031AB - 0.009AC - 0.013AD \\ & - 0.0027BC + 0.0035BD - 0.0137CD \\ & + 0.0148A^2 + 0.0246B^2 + 0.009C^2 + 0.0011D^2\end{aligned}$$

The regression coefficient value was high (R^2=0.9444), and the lack of fit was not significant, suggesting that the model is suitable for studying the formulation of CBD-NLCs. As shown in Figure 1B, the regression equation fit well with the experimental results, and the coefficients of each phase of the equation were statistically significant. Notably, when lambda equaled −0.59, the Box−Cox curve of power transformation reached the minimum value. The perturbation plot of Figure 1B shows the influence of each variable on PDI. The influence of each variable on PDI is as follows: B (lipid concentration) > A (solid−liquid lipid ratio) > C (surfactant concentration) > D (CBD concentration). The effects of solid−liquid lipid ratio and lipid concentration on PDI were extremely significant. An appropriate ratio and concentration resulted in a uniform structure with low PDI values. Conversely, inadequate or excessive lipid concentrations led to particle clusters with varying sizes and shapes, resulting in an inhomogeneous final formulation. Furthermore, increasing surfactant concentration also elevated PDI levels due to the substantial accumulation of surfactant on the NLC surface, which affected the size and distribution of particles.

3.1.3. Effects on EE. EE significantly affects the release characteristics of the NLCs. The release of the embedded substance is achieved through the diffusion and degradation of the coated lipid particles. Among all 29 experimental runs, the EE values for CBD-NLCs varied from 78.08 ± 1.76 to 90.24 ± 0.57%. Figure S4 shows a 3D surface responses of the variable's impact on EE. The mathematical equation presented below elucidates how various variables impact the EE of CBD-NLCs:

$$\begin{aligned}\text{EE} = {} & + 86.96 + 2.49A + 2.82B - 0.5783C - 0.3283D \\ & + 0.22AB - 0.5925AC - 0.22AD - 2.02BC \\ & - 2.66BD + 1.4CD - 0.7895A^2 - 1.73B^2 \\ & - 0.7008C^2 - 1.69D^2\end{aligned}$$

The regression coefficient value was high (R^2=0.9613), and the lack of fit was not significant, which signifies a good fit of the model. As demonstrated in Figure 1C, the predicted and actual values fit well. Additionally, when the lambda was 0.86, the Box−Cox curve of power transformation reached the minimum value. Furthermore, based on the two-dimensional perturbation plot of Figure 1C, it can be seen that the variables have different influences on EE. The influence of each variable on EE is as follows: B (lipid concentration) > A (solid−liquid lipid ratio) > C (surfactant concentration) > D (CBD concentration). Notably, the lipid concentration plays a crucial role in determining EE due to its influence on CBD solubility.

3.2. Optimization. The optimal formulation conditions for CBD-NLCs were determined using a multiresponse surface method, considering particle size, PDI, and EE. Several criteria were set for the dependent variable (Table 1): minimize the particle size and PDI while maximizing EE. The individual desirability functions were finally combined through an extensive grid and feasibility search across the domain, resulting in the global desirability value using the Design Expert 11 software as a function of geometric mean.[46] The predicted values can be clearly seen in Figure S6. The optimum CBD-NLC formulation conditions were as follows: solid−liquid lipid ratio was 1.28 (w/w), lipid concentration was 1.95 (w/v), surfactant concentration was 2.93 (w/v), and CBD concentration was 1.04 (*w/v*). To verify the applicability of the model, three execution batches of CBD-NLCs were prepared under these conditions. The confirmed results of optimal conditions were close to predicted values (Table 4).

3.3. Characterization of NLCs. *3.3.1. Particle Size, PDI, Zeta Potential, and Morphology Analysis.* The morphology of CBD-NLCs was observed by SEM and TEM (Figure 2). The particle size and zeta potential distribution are shown in Figure S5. The results revealed that CBD-NLCs exhibited a nearly

https://doi.org/10.1021/acsomega.4c04771
ACS Omega 2024, 9, 40632−40643

Table 4. Predicted Value of the Independent Variables and Comparison of Actual and Predicted Values in the CBD-NLCs

response independent variables	predicted values	actual values	residual (%)
particle size (nm)	56.66	54.33 ± 1.11	2.05
PDI	0.119	0.118 ± 0.003	2.24
EE (%)	87.33	87.58 ± 1.57	1.79

spherical shape with uniform particle size distribution. The average particle size was approximately 60 nm, which showed slight variation compared to the DLS measurements. This discrepancy arises from the surface coating of gold with a thickness of 6−9 nm on the NLCs to enhance their conductivity prior to TEM, resulting in an increase in the average particle diameter.

3.3.2. FTIR Analysis. The FTIR spectra of CBD-NLCs, physical mixtures, P188, GML, and CBD are shown in Figure 3. The spectra of CBD showed several characteristic peaks, including methyl and methylene groups at 2920 cm^{-1}, carbon double bonds at approximately 1620 and 1580 cm^{-1}, as well as phenolic hydroxyls and benzene C−H bonds at approximately 1210 and 1020 cm^{-1}, respectively.[47] The bands observed in the CBD-NLCs and physical mixture spectra were generally consistent with those in the P188 and GML spectra. Moreover, compared with those in the P188 spectrum, the bands at approximately 1330, 1000, and 835 cm^{-1} attenuated after NLC formation, which corresponded to the long-chain saturated hydrocarbon sec-carbon backbone and C−H bonds in the hydrophobic block. The ether bond signals belonging to the hydrophilic block around 1100 cm^{-1} were still evident. Notably, compared to the physical mixture, the characteristic peaks of CBD diminished in the CBD-NLC spectra, suggesting that a large amount of CBD was embedded within the lipid bilayer relative to the NLC surface.

3.3.3. Thermal Analysis. DSC studies were conducted to investigate the crystallinity of NLCs and the interaction between the drug and lipid in the formulation. The DSC thermograms of CBD-NLCs, the physical mixture, P188, GML and CBD are shown in Figure 4. The DSC curves of P188, GML, and CBD displayed a single endothermic event at temperatures of 57.87, 65.03, and 64.30 °C, respectively. In addition, the physical mixture showed a lower melting temperature compared to P188, GML, and CBD due to the smaller particle size produced by grinding during the mixing process. It can be clearly seen that the

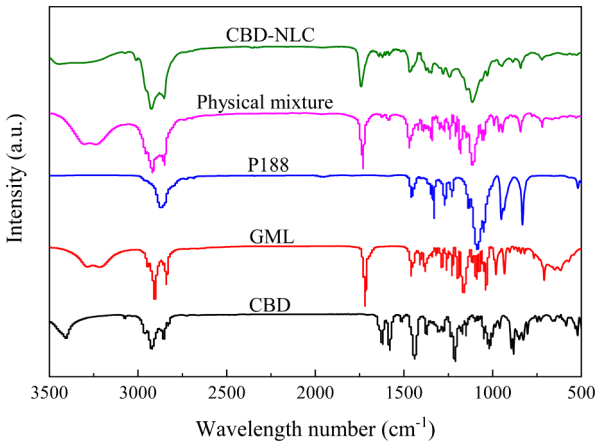

Figure 3. FTIR spectra of CBD-NLCs, the physical mixture, P188, GML, and CBD.

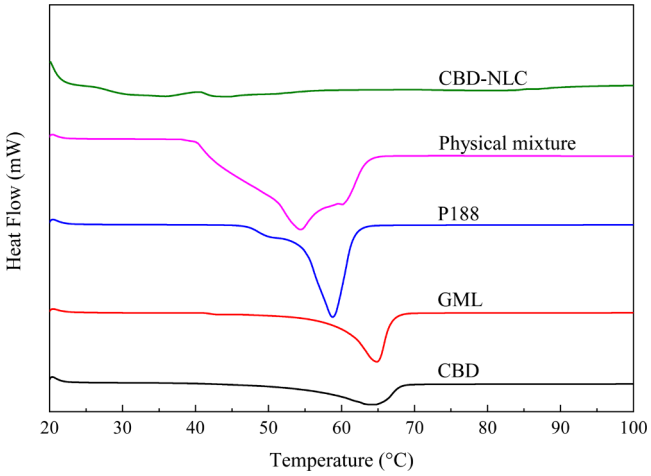

Figure 4. DSC thermogram of CBD-NLCs, the physical mixture, P188, GML, and CBD.

DSC curve of CBD-NLCs exhibited the lowest melting point and the widest range of peaks among all the curves, and there was no heat-absorption peak of CBD. The change in melting point may be due to the interaction between solid and liquid lipids during preparation, resulting in a more disordered and imperfect crystal structure, further confirming the loading of CBD in NLCs.

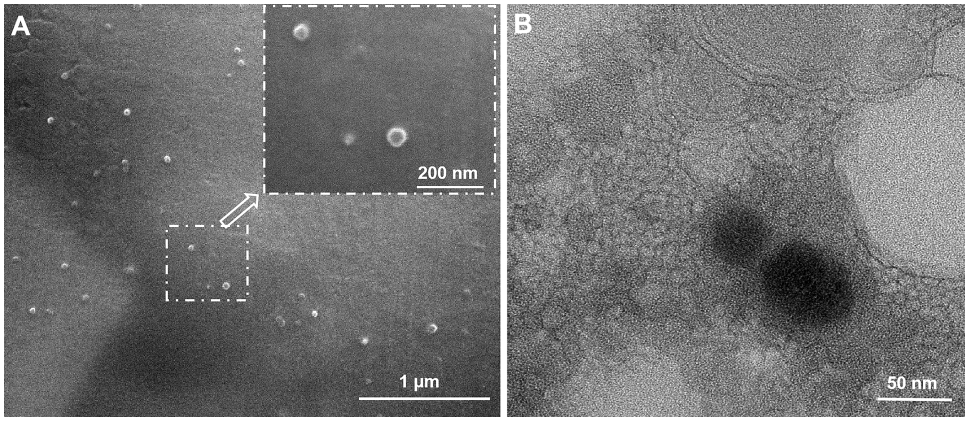

Figure 2. Morphology of the optimum formulation of CBD-NLCs: (A) SEM images and (B) TEM image.

https://doi.org/10.1021/acsomega.4c04771
ACS Omega 2024, 9, 40632−40643

3.3.4. XRD Analysis. The crystallinity of CBD-NLCs, the physical mixture, P188, GML, and CBD were examined using XRD measurements. As shown in Figure 5, the main peaks found for CBD (9.64, 10.17, 17.42, 18.78, and 22.17° 2θ), GML (9.57 and 10.30° 2θ), and P188 (19.05, 20.57, and 23.25° 2θ) showed that these compounds had a crystalline nature. It is evident that some of the characteristic crystalline peaks of P188, GML, and CBD can still be observed in the physical mixture, whereas the characteristic crystalline peaks disappeared in the spectra of CBD-NLCs, suggesting that CBD was in the noncrystalline state.

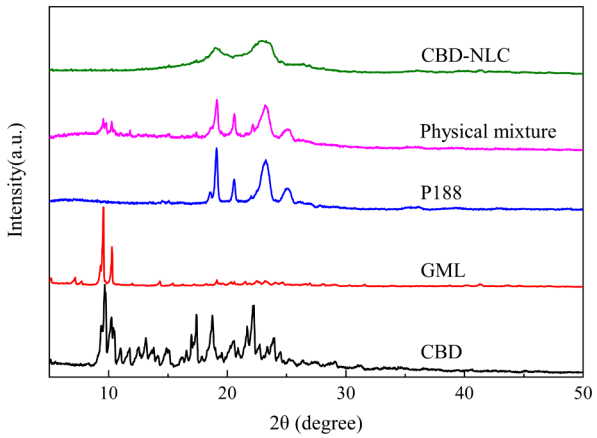

Figure 5. XRD pattern of CBD-NLCs, the physical mixture, P188, GML, and CBD.

3.4. Stability of CBD-NLCs. *3.4.1. Ionic and pH Stability.* The human digestive system contains many kinds of salt, especially sodium and calcium salt. It should be noted that the salt concentration may affect the stability of the delivery system. The effects of different concentrations of NaCl and $CaCl_2$ on CBD-NLCs are shown in Figure 6A,B. No aggregation or color change was evident in the appearance of all samples. When the concentration of NaCl was less than 50 mmol, the particle size of the NLCs barely changed. As the concentration continued to increase, the particle size increased slightly. The addition of NaCl reduced the PDI to less than 0.1, indicating that the system was uniform and stable. The reason for this phenomenon may be that the addition of NaCl enhanced the strength of ions in the system, reduced the proximity frequency of the particles, and improved the stability of the system, suggesting that CBD-NLCs had a good tolerance to NaCl. Likewise, when the concentration of $CaCl_2$ was lower than 50 mmol, the particle size did not change significantly and the PDI was lower than the initial value, whereas when the concentration was above 100 mmol, the particle size increased significantly and the PDI increased rapidly. Compared with NaCl, the addition of $CaCl_2$ had more obvious effects on the particle size and PDI of the CBD-NLCs. It can be found that $CaCl_2$ can make NLCs overcome the potential barrier and produce rapid aggregation at lower concentrations, which may be due to the superior negative charge neutralization of divalent calcium ions over monovalent sodium ions on the surface of NLCs. In addition, Ca^{2+} can form a "salt bridge" between the NLCs and increase the hydrophobicity of the phospholipid membrane, leading to the instability of the NLCs.

NLCs may experience different pH conditions in food formulations or the human digestive system; therefore, their

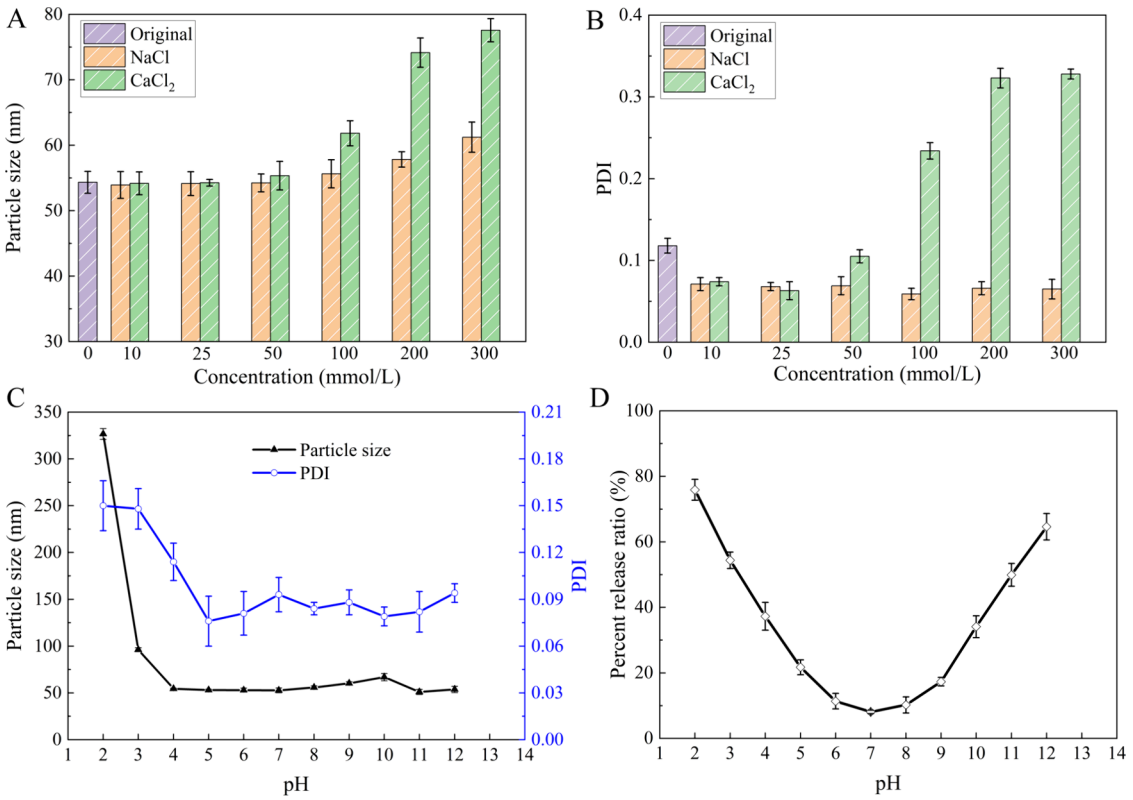

Figure 6. (A, B) The effects of different concentrations of NaCl and $CaCl_2$ on particle size and PDI of CBD-NLCs. (C) The effects of pH on particle size and PDI. (D) The effects of pH on the percent release ratio.

https://doi.org/10.1021/acsomega.4c04771
ACS Omega 2024, 9, 40632−40643

pH stability is critical. The effects of different pH conditions on CBD-NLCs were investigated. The particle size remained relatively stable within the pH range of 4 to 12, as depicted in Figure 6A. However, when pH was less than 4, the samples became turbid, and the particle size increased rapidly along with the increase in PDI. Changes in pH had a strong impact on the percent release ratio of CBD from NLCs. The CBD release ratio was consistently below 20% within the pH range of 6 to 9, with a minimum value (8.08 ± 0.55%) observed at pH 7, indicating that CBD is more stable in a neutral environment. It is worth noting that the color of the samples turned pink when the pH reached above 10, and the color deepened with an increase in pH, which may be due to the reaction or degradation of the released CBD under strong alkaline conditions.

3.4.2. UV Irradiation Stability. CBD is reported to be easily photodegraded, which has an important effect on its biological activity.[48] Figure 7 shows the UV stability of free CBD and CBD-NLCs. The experimental results revealed that UV irradiation exerted a substantial influence on the retention rate of CBD. The free CBD was degraded over 50% in 90 min. The results validate that CBD exhibits a pronounced photosensitivity attributed to the UV absorption capacity of the aromatic ring. However, when encapsulated in NLCs, the preservation rate of CBD significantly increases to approximately 90% and remained relatively stable during 90 min of exposure to UV with minimal fluctuations. These findings demonstrate that the CBD-NLCs were an effective system to avoid the photochemical degradation of CBD. The cladding formation enhances the physical barrier, effectively hindering the transmission of UV and minimizing CBD exposure.

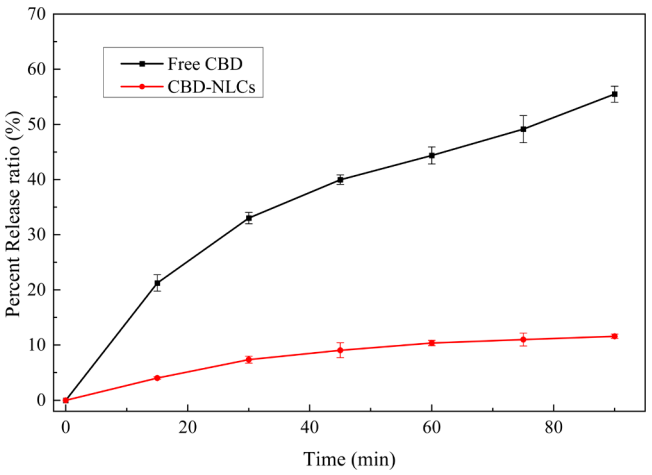

Figure 7. UV stability of free CBD and CBD-NLCs.

3.4.3. Thermal Stability. As an effective carrier for CBD, the integrity of the carriers is very important during heat treatment. Elevated temperatures may induce a structural transition in NLCs, leading to conversion from an initial disordered state to an ordered configuration, consequently resulting in drug leakage and degradation. The results showed that the particle size and PDI of CBD-NLCs remained relatively stable at 4, 25, 37, and 60 °C (Figure 8A). However, when subjected to a temperature of 80 °C for 1.5 h, the particle size increased by approximately 10%, whereas the PDI increased by nearly 15% (Figure 8A). The effect of the temperature on the percent release ratio of CBD is shown in Figure 8. As the system was heated, there was a gradual increase in CBD leakage. According to the results, the percent release rate of CBD-NLCs was relatively low and stable at 4−37 °C (Figure 8B). Therefore, it is recommended to store CBD-NLCs at a lower temperature.

3.4.4. Storage Stability. During long-term storage, NLCs may degrade or aggregate, leading to the release of the encapsulated compound. Figure 9 represents the impact of storage period on particle size, PDI, and release rate of CBD-NLCs. As can be seen in Figure 9, the particle size of CBD-NLCs increased at both storage temperatures, indicating that the interparticle repulsive forces decreased with storage time, causing the particles to aggregate. Notably, the extent of change in particle size was comparatively smaller at 4 °C, implying that lower temperature conditions are more favorable for long-term preservation of CBD-NLCs. The results presented in Figure 9 demonstrated that even after a period of 42 days, CBD-NLCs exhibited an impressive retention rate of over 78% CBD, indicating its remarkable ability to effectively prevent degrada-

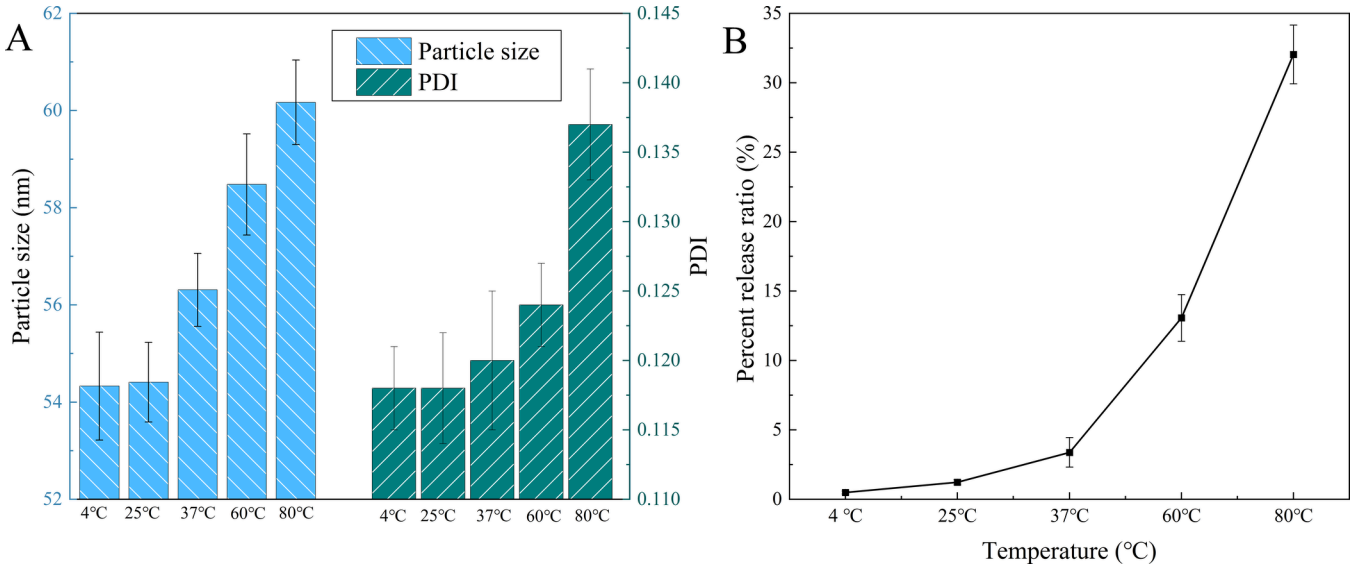

Figure 8. (A) Particle size and PDI of CBD-NLCs at different temperature. (B) The percent release ratio of CBD-NLCs at different temperatures.

https://doi.org/10.1021/acsomega.4c04771
ACS Omega 2024, 9, 40632−40643

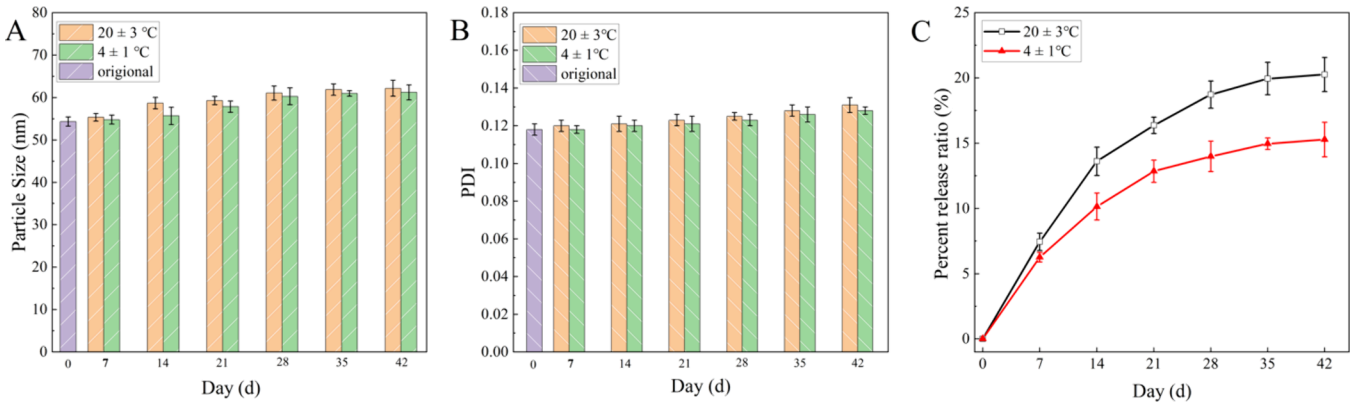

Figure 9. Impact of storage period of CBD-NLCs: (A) particle size, (B) PDI, and (C) release rate.

tion during the storage process. These findings highlight the practical significance of CBD-NLCs for the food industry.

3.5. In Vitro Release Study. The cumulative release profiles of CBD and CBD-NLCs were evaluated over 180 min, as depicted graphically in Figure 10. It can be clearly seen that

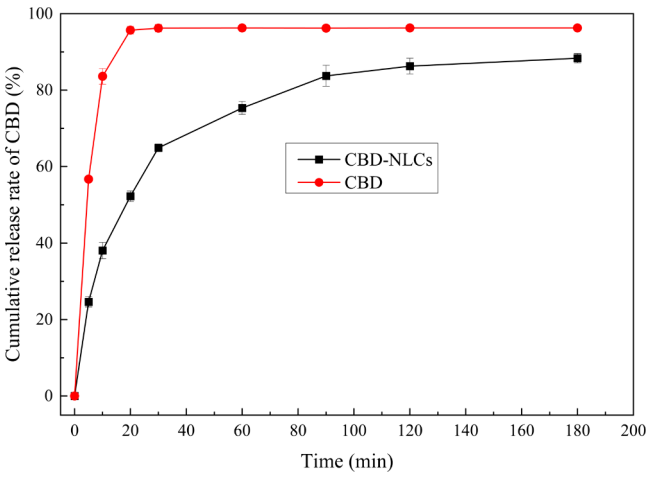

Figure 10. CBD release profiles from CBD and CBD-NLCs.

CBD-NLCs exhibited a biphasic release profile characterized by an initial burst release (over 50% of CBD released within 20 min) followed by a subsequent gradual and sustained release. This release pattern with two distinct phases has been previously reported for NLCs.[49,50] This is related to the diffusion of CBD from the lipid matrix of the NLCs and its location within the lipid matrix. During the preparation of NLCs, a rapid decrease in the temperature was required to cool the lipid; however, this rapid cooling resulted in partial encapsulation of CBD within the outer layer of the NLCs. When NLCs were placed in PBS containing P188, CBD of the outer layer was rapidly released, leading to an initial burst release. The subsequent sustained release can be attributed to the interaction between CBD encapsulated within the NLCs and the lipid matrix.[51] The biphasic release profile is especially beneficial for diseases such as cancer, where the initial burst release provides a direct and potent dose followed by sustained drug delivery at the tumor site. Otherwise, the small size of the prepared CBD-NLCs, measuring only a few tens of nanometers in dimension, results in a significantly increased surface area and consequently leads to an accelerated release rate.[52]

The CBD release data were analyzed using various mathematical models listed in Table 5 and Figure S7 to identify

Table 5. In Vitro Kinetic Modeling Release Fitting Results of CBD-NLCs

modeling	fitting equation	R^2
zero-order formula	$Q_t = 33.72t + 0.41$	0.6159
first-order formula	$Q_t = 84.61(1 - e^{-0.05t})$	0.9851
Higuchi formula	$Q_t = 6.62t^{1/2} + 15.18$	0.8714
Ritger−Peppas formula	$Q_t = 21.34t^{0.29}$	0.9583

the most suitable model for describing the drug release kinetics. The results showed that the best fitting equation for the in vitro release of CBD-NLCs is the first-order equation (R^2=0.9851, Figure S7B), suggesting that the mechanism of CBD-NLC release is a process of controlling drug release with the initial concentration. Furthermore, the Ritger−Peppas model supported these findings, with an n value of 0.29 (less than 0.45), which is classified as Fickian diffusion. The phenomenon of Fickian diffusion is characterized by an initial rapid release followed by a gradual decrease over time. The mechanism underlying this release involves the process of chemical gradient-driven diffusion.

4. CONCLUSIONS

The formulation of CBD-loaded NLCs was developed, optimized, and characterized. The optimal formulation proposed by RSM-BBD resulted in a particle size of 54.33 nm, a PDI of 0.118, a zeta potential of −29.7 mV, and an EE of 87.58%, indicating a uniform particle size distribution, physical stability, and high encapsulation efficiency. The CBD-NLCs exhibited a nearly spherical shape with uniform particle size distribution. FTIR, DSC, and XRD results confirmed effective encapsulation of CBD within the NLC structure rather than simple physical mixing with lipids and surfactants. The stability experiments demonstrated that CBD-NLCs exhibited enhanced tolerance to N^{a+} compared to Ca^{2+} while remaining relatively stable within pH levels ranging from 6 to 9. Additionally, the NLC structure effectively mitigates the photodegradation of CBD and enhances its thermal stability. The particle size and PDI of CBD-NLCs remained relatively stable under temperatures ranging from 4 to 60 °C, with CBD leakage below 5% at temperatures between 4 and 37 °C. Furthermore, it was observed that the prepared CBD-NLCs did not exhibit noticeable aggregation after being stored for 42 days, with a retention rate exceeding 78%. In vitro release experiments

https://doi.org/10.1021/acsomega.4c04771
ACS Omega 2024, 9, 40632−40643

revealed a biphasic release profile characterized by an initial burst release of CBD, with over 50% released within 20 min, followed by a subsequent gradual and sustained release consistent with a first-order kinetics model.

The water solubility of CBD is enhanced by this formulation, and its stability is satisfactory; however, the observed burst release in CBD-NLCs still persists, which is closely associated with the absorption, distribution, and metabolism kinetics of CBD in the human body. Therefore, further investigations are warranted to enhance the sustained release of CBD-NLCs, such as additional adjustments of formulation, secondary coating, and so on.

■ ASSOCIATED CONTENT

Supporting Information

The Supporting Information is available free of charge at https://pubs.acs.org/doi/10.1021/acsomega.4c04771.

> Optimization of the solid lipid, liquid lipid, and surfactant; kinetic equations; HPLC standard curve; 3D response surface plots; size distribution and zeta potential distribution; overlay plot; and in vitro kinetic modeling release fitting results (DOCX)

■ AUTHOR INFORMATION

Corresponding Author

Yang Xie − *Heilongjiang Academy of Sciences, Institute of Advanced Technology, Harbin 150020, China;* orcid.org/0000-0001-9337-8763; Email: xyy89650641@126.com

Authors

Peng Li − *Heilongjiang Academy of Sciences, Institute of Advanced Technology, Harbin 150020, China*

Dong Fu − *Heilongjiang Academy of Sciences, Institute of Advanced Technology, Harbin 150020, China*

Fan Yang − *Heilongjiang Academy of Sciences, Institute of Advanced Technology, Harbin 150020, China*

Xin Sui − *Heilongjiang Academy of Sciences, Institute of Advanced Technology, Harbin 150020, China*

Bo Huang − *Heilongjiang Academy of Sciences, Institute of Advanced Technology, Harbin 150020, China;* orcid.org/0000-0003-0911-5739

Jiaying Liu − *Heilongjiang Academy of Sciences, Institute of Advanced Technology, Harbin 150020, China*

Jialong Chi − *Heilongjiang Academy of Sciences, Institute of Advanced Technology, Harbin 150020, China*

Complete contact information is available at: https://pubs.acs.org/10.1021/acsomega.4c04771

Notes

The authors declare no competing financial interest.

■ ACKNOWLEDGMENTS

This work was supported by the Heilongjiang Academy of Science (KY2023GJS03).

■ REFERENCES

(1) Matarazzo, A. P.; Elisei, L. M. S.; Carvalho, F. C.; Vonfílio, R.; Ruela, A. L. M.; Galdino, G.; Pereira, G. R. Mucoadhesive Nanostructured Lipid Carriers as a Cannabidiol Nasal Delivery System for the Treatment of Neuropathic Pain. *Eur. J. Pharm. Sci.* **2021**, *159* (4), No. 105698.

(2) Hasbi, A.; Madras, B. K.; George, S. R. Endocannabinoid System and Exogenous Cannabinoids in Depression and Anxiety: A Review. *Brain Sci.* **2023**, *13* (2), 325.

(3) Hill, M. N.; Hillard, C. J.; Bambico, F. R.; Patel, S.; Gorzalka, B. B.; Gobbi, G. The Therapeutic Potential of the Endocannabinoid System for the Development of a Novel Class of Antidepressants. *Trends Pharmacol. Sci.* **2009**, *30* (9), 484−493.

(4) Sarris, J.; Sinclair, J.; Karamacoska, D.; Davidson, M.; Firth, J. Medicinal Cannabis for Psychiatric Disorders: A Clinically-focused Systematic Review. *BMC Psychiatry* **2020**, *20*, 24.

(5) Poleszak, E.; Wośko, S.; Sławińska, K.; Szopa, A.; Wróbel, A.; Serefko, A. Cannabinoids in Depressive Disorders. *Life Sci.* **2018**, *213*, 18−24.

(6) Yarar, E. Role and Function of Endocannabinoid System in Major Depressive Disease. *Med. Cannabis Cannabinoids* **2021**, *4* (1), 1−12.

(7) Li, H.; Chang, S. L.; Chang, T. R.; You, Y.; Wang, X. D.; Wang, L. W.; Yuan, X. F.; Tan, M. H.; Wang, P. D.; Xu, P. W.; Gao, W. B.; Zhao, Q. S.; Zhao, B. Inclusion Complexes of Cannabidiol with β-cyclodextrin and Its Derivative: Physicochemical Properties, Water Solubility, and Antioxidant Activity. *J. Mol. Liq.* **2021**, *334*, No. 116070.

(8) Štukelj, R.; Benčina, M.; Fanetti, M.; Valant, M.; Drab, M.; Iglič, A.; Kralj-Iglič, V. Synthesis of Stable Cannabidiol (CBD) Nanoparticles in Suspension. *Mater. Technol.* **2019**, *53*, 543−549.

(9) Gáll, Z.; Farkas, S.; Albert, Á.; Ferencz, E.; Vancea, S.; Urkon, M.; Kolcsár, M. Effects of Chronic Cannabidiol Treatment in the Rat Chronic Unpredictable Mild Stress Model of Depression. *Biomolecules* **2020**, *10* (5), 801.

(10) Kopustinskiene, D. M.; Masteikova, R.; Lazauskas, R.; Bernatoniene, J. *Cannabis sativa* L. Bioactive Compounds and Their Protective Role in Oxidative Stress and Inflammation. *Antioxidants* **2022**, *11*, 660.

(11) Watt, G.; Karl, T. In vivo Evidence for Therapeutic Properties of Cannabidiol (CBD) for Alzheimer's Disease. *Front. Pharmacol.* **2017**, *8*, 20.

(12) Shannon, S.; Lewis, N.; Lee, H.; Hughes, S. Cannabidiol in Anxiety and Sleep: a Large Case Series. *Perm. J.* **2019**, *23*, 18−41.

(13) García-Gutiérrez, M. S.; Navarrete, F.; Gasparyan, A.; Austrich-Olivares, A.; Sala, F.; Manzanares, J. Cannabidiol: a Potential New Alternative for the Treatment of Anxiety, Depression, and Psychotic Disorders. *Biomolecules* **2020**, *10* (11), 1575.

(14) Knaub, K.; Sartorius, T.; Dharsono, T.; Wacker, R.; Wilhelm, M.; Schön, C. A Novel Self-Emulsifying Drug Delivery System (SEDDS) Based on VESIsorb Formulation Technology Improving the Oral Bioavailability of Cannabidiol in Healthy Subjects. *Molecules* **2019**, *24* (16), 2967.

(15) Ahmed, M.; Boileau, I.; Le Foll, B.; Carvalho, A. F.; Kloiber, S. The Endocannabinoid System in Social Anxiety Disorder: From Pathophysiology to Novel Therapeutics. *Braz. J. Psychiatry* **2022**, *44*, 81−93.

(16) Hasbi, A.; Madras, B. K.; George, S. R. Endocannabinoid System and Exogenous Cannabinoids in Depression and Anxiety: A Review. *Brain Sci.* **2023**, *13*, 325.

(17) Koch, N.; Jennotte, O.; Gasparrini, Y.; Vandenbroucke, F.; Lechanteur, A.; Evrard, B. Cannabidiol Aqueous Solubility Enhancement: Comparison of Three Amorphous Formulations Strategies Using Different Type of Polymers. *Int. J. Pharm.* **2020**, *589*, No. 119812.

(18) Cherniakov, I.; Izgelov, D.; Domb, A. J.; Hoffman, A. The Effect of Pro NanoLipospheres (PNL) Formulation Containing Natural Absorption Enhancers on the Oral Bioavailability of Delta-9-tetrahydrocannabinol (THC) and Cannabidiol (CBD) in a Rat Model. *Eur. J. Pharm. Sci.* **2017**, *109*, 21−30.

(19) Sitovs, A.; Logviss, K.; Lauberte, L.; Mohylyuk, V. Oral Delivery of Cannabidiol: Revealing the Formulation and Absorption Challenges. *J. Drug. Delivery Sci. Tec.* **2024**, *92*, No. 105316.

(20) Franco, V.; Gershkovich, P.; Perucca, E.; Bialer, M. The Interplay Between Liver First-Pass Effect and Lymphatic Absorption of Cannabidiol and Its Implications for Cannabidiol Oral Formulations. *Clin. Pharmacokinet.* **2020**, *59* (12), 1493−1500.

(21) Grifoni, L.; Vanti, G.; Donato, R.; Sacco, C.; Bilia, A. R. Promising Nanocarriers to Enhance Solubility and Bioavailability of Cannabidiol for a Plethora of Therapeutic Opportunities. *Molecules* **2022**, *27* (18), 6070.
(22) Xu, L.; Wang, X.; Liu, Y.; Yang, G.; Falconer, R. J.; Zhao, C. X. Lipid Nanoparticles for Drug Delivery. *Adv. NanoBiomed Res.* **2022**, *2*, 2100109.
(23) Chu, P. C.; Liao, M. H.; Liu, M. G.; Li, C. Z.; Lai, P. S. Key Transdermal Patch Using Cannabidiol-Loaded Nanocarriers with Better Pharmacokinetics in vivo. *Int. J. Nanomed.* **2024**, *19*, 4321−4337.
(24) Tijani, A. O.; Thakur, D.; Mishra, D.; Frempong, D.; Chukwunyere, U. I.; Puri, A. Delivering Therapeutic Cannabinoids via Skin: Current State and Future Perspectives. *J. Controlled Release* **2021**, *334*, 427−451.
(25) Patrician, A.; Versic-Bratincevic, M.; Mijacika, T.; Banic, I.; Marendic, M.; Sutlović, D.; Dujić, Ž.; Ainslie, P. N. Examination of a New Delivery Approach for Oral Cannabidiol in Healthy Subjects: A Randomized, Double-Blinded. *Placebo-Controlled Pharmacokinetics Study. Adv. Ther.* **2019**, *36* (11), 3196−3210.
(26) Crowley, K.; De Vries, S. T.; Moreno-Sanz, G. Self-Reported Effectiveness and Safety of Trokie Lozenges: A Standardized Formulation for the Buccal Delivery of Cannabis Extracts. *Front. Neurosci.* **2018**, *12*, 564.
(27) Söpper, U.; Hoffmann, A.; Daniels, R. Mucoadhesion and Mucopenetration of Cannabidiol (CBD)-Loaded Mesoporous Carrier Systems for Buccal Drug Delivery. *Sci. Pharm.* **2021**, *89* (3), 35.
(28) Atsmon, J.; Heffetz, D.; Deutsch, L.; Deutsch, F.; Sacks, H. Single-Dose Pharmacokinetics of Oral Cannabidiol Following Administration of PTL101: A New Formulation Based on Gelatin Matrix Pellets Technology. *Clin. Pharmacol. Drug Dev.* **2018**, *7* (7), 751−758.
(29) Kaplan, B. L. F.; Swanson, E. A.; Ross, M. K.; Olivier, A. K.; Guo-Ross, S. X.; Burroughs, K. J.; Ross, A. K.; Matula, M.; Tarbox, T.; Greenberg, M.; Carr, R. L. Nanochannel Delivery System for CBD: Sustained Low Level Plasma Levels without Liver Toxicity. *J. Drug Delivery Sci. Tec.* **2023**, *79*, No. 104029.
(30) Zapata, K.; Rosales, S. R.; Rios, A.; Rojano, B.; Toro-Mendoza, J.; Riazi, M.; Franco, C. A.; Cortés, F. B. Nanoliposomes for Controlled Release of Cannabinodiol at Relevant Gastrointestinal Conditions. *ACS Omega* **2023**, *8* (46), 43698−43707.
(31) Akbari, J.; Saeedi, M.; Ahmadi, F.; Hashemi, H. S. M.; Babaei, A.; Yaddollahi, S.; Rostamkalaei, S. S.; Asare-Addo, K.; Nokhodchi, A. Solid Lipid Nanoparticles and Nanostructured Lipid Carriers: a Review of the Methods of Manufacture and Routes of Administration. *Pharm. Dev. Technol.* **2022**, *27* (5), 525−544.
(32) Chutoprapat, R.; Kopongpanich, P.; Chan, L. W. A Mini-Review on Solid Lipid Nanoparticles and Nanostructured Lipid Carriers: Topical Delivery of Phytochemicals for the Treatment of *Acne Vulgaris*. *Molecules* **2022**, *27* (11), 3460.
(33) Perucca, E.; Bialer, M. Critical Aspects Affecting Cannabidiol Oral Bioavailability and Metabolic Elimination, and Related Clinical Implications. *CNS Drugs* **2020**, *34* (8), 795−800.
(34) Viegas, C.; Patrício, A. B.; Prata, J. M.; Nadhman, A.; Chintamaneni, P. K.; Fonte, P. Solid Lipid Nanoparticles vs.Nanostructured Lipid Carriers: A Comparative Review. *Pharmaceutics* **2023**, *15*, 1593.
(35) Zielińska, A.; da Ana, R.; Fonseca, J.; Szalata, M.; Wielgus, K.; Fathi, F.; Oliveira, M. B. P. P.; Staszewski, R.; Karczewski, J.; Souto, E. B. Phytocannabinoids: Chromatographic Screening of Cannabinoids and Loading into Lipid Nanoparticles. *Molecules* **2023**, *28* (6), 2875.
(36) Faiz, S.; Arshad, S.; Kamal, Y.; Imran, S.; Asim, M. H.; Mahmood, A.; Inam, S.; Irfan, H. M.; Riaz, H. Pioglitazone-Loaded Nanostructured Lipid Carriers: In-vitro and in-vivo Evaluation for Improved Bioavailability. *J. Drug Delivery Sci. Tec.* **2023**, *79*, No. 104041.
(37) Syed Azhar, S. N. A.; Ashari, S. E.; Zainuddin, N.; Hassan, M. Nanostructured Lipid Carriers-Hydrogels System for Drug Delivery: Nanohybrid Technology Perspective. *Molecules* **2022**, *27* (1), 289.
(38) Vishwakarma, N.; Jain, A.; Sharma, R.; Mody, N.; Vyas, S.; Vyas, S. P. Lipid-Based Nano-Carriers for Lymphatic Transportation. *AAPS PharmSciTech* **2019**, *20* (2), 83−96.
(39) Agarwal, S.; Kumar, S.; Garg, R. Investigative Study on Impact of Solid: Liquid Lipid Ratio and Stabilizer Amount on Some Characteristics of Nanostructure Lipid Carriers of Quetiapine Fumarate. *Int. J. Pharma. Investig.* **2019**, *9* (2), 47−52.
(40) Vardanega, R.; Lüdtke, F. L.; Loureiro, L.; Toledo Hijo, A. A. C.; Martins, J. T.; Pinheiro, A. C.; Vicente, A. A. Enhancing Cannabidiol Bioaccessibility Using Ionic Liquid as Emulsifier to Produce Nanosystems: Characterization of Structures, Cytotoxicity Assessment, and in vitro Digestion. *Food Res. Int.* **2024**, *188*, No. 114498.
(41) Amasya, G.; Ergin, A. D.; Cakirci, O. E.; Ozçelikay, A. T.; Bayindir, Z. S.; Yuksel, N. A Study to Enhance the Oral Bioavailability of s-adenosyl-l-methionine (SAMe): SLN and SLN Nanocomposite Particles. *Chem. Phys. Lipids* **2021**, *237*, No. 105086.
(42) Morakul, B.; Junyaprasert, V. B.; Sakchaisri, K.; Teeranachaideekul, V. Cannabidiol-Loaded Nanostructured Lipid Carriers (NLCs) for Dermal Delivery: Enhancement of Photostability, Cell Viability, and Anti-Inflammatory Activity. *Pharmaceutics* **2023**, *15*, 537.
(43) Vardanega, R.; Lüdtke, F. L.; Loureiro, L.; Goncalves, R. F. S.; Pinheiro, A. C.; Vicente, A. A. Development and characterization of nanostructured lipid carriers for cannabidiol delivery. *Food Chem.* **2024**, *441*, No. 138295.
(44) Ferron, L.; Milanese, C.; Colombo, R.; Pugliese, R.; Papetti, A. Selection and Optimization of an Innovative Polysaccharide-Based Carrier to Improve Anthocyanins Stability in Purple Corn Cob Extracts. *Antioxidants* **2022**, *11*, 916.
(45) Moqejwa, T.; Marimuthu, T.; Kondiah, P. P. D.; Choonara, Y. E. Development of Stable Nano-Sized Transfersomes as a Rectal Colloid for Enhanced Delivery of Cannabidiol. *pharmaceutics* **2022**, *14* (4), 703.
(46) Ashar, F.; Hani, U.; Osmani, R. A. M.; Kazim, S. M.; Selvamuthukumar, S. Preparation and Optimization of Ibrutinib-Loaded Nanoliposomes Using Response Surface Methodology. *Polymers* **2022**, *14*, 3886.
(47) Vardanega, R.; Lüdtke, F. L.; Loureiro, L.; Gonçalves, R. F. S.; Pinheiro, A. C.; Vicente, A. A. Development and Characterization of Nanostructured Lipid Carriers for Cannabidiol Delivery. *Food Chem.* **2024**, *441*, No. 138295.
(48) Seccamani, P.; Franco, C.; Protti, S.; Porta, A.; Profumo, A.; Caprioglio, D.; Salamone, S.; Mannucci, B.; Merli, D. Photochemistry of Cannabidiol (CBD) Revised. A Combined Preparative and Spectrometric Investigation. *J. Nat. Prod.* **2021**, *84* (11), 2858−2865.
(49) Mendes, I. T.; Ruela, A. L. M.; Carvalho, F. C.; Freitas, J. T. J.; Bonfilio, R.; Pereira, G. R. Development and Characterization of Nanostructured Lipid Carrier-Based Gels for the Transdermal Delivery of Donepezil. *Colloid. Surface B* **2019**, *177*, 274−281.
(50) Qushawy, M.; Nasr, A.; Abd-Alhaseeb, M.; Swidan, S. A. Design, Optimization and Characterization of a Transfersomal Gel Using Miconazole Nitrate for the Treatment of Candida Skin Infections. *Pharmaceutics* **2018**, *10* (1), 26.
(51) Grifoni, L.; Vanti, G.; Donato, R.; Sacco, C.; Bilia, A. R. Promising Nanocarriers to Enhance Solubility and Bioavailability of Cannabidiol for a Plethora of Therapeutic Opportunities. *Molecules* **2022**, *27*, 6070.
(52) Reddy, T. S.; Zomer, R.; Mantri, N. Nanoformulations as a strategy to overcome the delivery limitations of cannabinoids. *Phytother. Res.* **2023**, *37*, 1526.

https://doi.org/10.1021/acsomega.4c04771
ACS Omega 2024, 9, 40632−40643